THE JOURNAL OF PHYSICAL CHEMISTRY B

Article

pubs.acs.org/JPCB

Incisive Probing of Intermolecular Interactions in Molecular Crystals: Core Level Spectroscopy Combined with Density Functional Theory

Joanna S. Stevens,[†] Che R. Seabourne,[‡] Cherno Jaye,[§] Daniel A. Fischer,[§] Andrew J. Scott,[‡] and Sven L. M. Schroeder*[,†,∥]

[†]School of Chemical Engineering and Analytical Science and [∥]School of Chemistry, The University of Manchester, Oxford Road, Manchester, M13 9PL, United Kingdom

[‡]Institute for Materials Research, School of Process, Environmental and Materials Engineering, University of Leeds, Leeds, LS2 9JT, United Kingdom

[§]National Institute of Standards and Technology, Gaithersburg, Maryland 20899, United States

Supporting Information

ABSTRACT: The α-form of crystalline *para*-aminobenzoic acid (PABA) has been examined as a model system for demonstrating how the core level spectroscopies X-ray photoelectron spectroscopy (XPS) and near-edge X-ray absorption fine-structure (NEXAFS) can be combined with CASTEP density functional theory (DFT) to provide reliable modeling of intermolecular bonding in organic molecular crystals. Through its dependence on unoccupied valence states NEXAFS is an extremely sensitive probe of variations in intermolecular bonding. Prediction of NEXAFS spectra by CASTEP, in combination with core level shifts predicted by WIEN2K, reproduced experimentally observed data very well when all significant intermolecular interactions were correctly taken into account. CASTEP-predicted NEXAFS spectra for the crystalline state were compared with those for an isolated PABA monomer to examine the impact of intermolecular interactions and local environment in the solid state. The effects of the loss of hydrogen-bonding in carboxylic acid dimers and intermolecular hydrogen bonding between amino and carboxylic acid moieties are evident, with energy shifts and intensity variations of NEXAFS features arising from the associated differences in electronic structure and bonding.

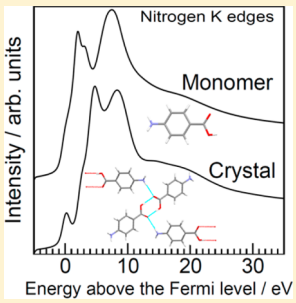

INTRODUCTION

Local molecular conformations and intermolecular bonding determine many physical properties of the organic solid state, including, for example, crystal structure, melting point, lattice energy and solubility. Physical properties influence, often cooperatively, more complex physicochemical behavior, such as the bioavailability of drugs.[1−3] Recent work has shown that core level spectroscopies, explicitly X-ray photoelectron spectroscopy (XPS)[4] and near edge X-ray absorption fine structure (NEXAFS),[5] can provide detailed insight into the underlying local chemical interactions and the electronic structure of molecular crystals.[6−14] They are very sensitive probes of hydrogen-bonding,[6,7,11,12,15−18] which has a strong effect on physical properties. To give one example, we have applied XPS to the characterization of crystalline organic materials,[7−10,19] distinguishing Brønsted proton transfer from hydrogen-bonding through chemical shifts in the nitrogen core level photoemission, and relating them to differences between the acidity constants of Brønsted donor and acceptor sites in two-component organic crystals.[7,8]

NEXAFS yields additional information through probing of unoccupied valence orbitals,[20] enabling incisive characterization of the local electronic state of functional groups and their interaction with other moieties in the solid. Interpretation of NEXAFS spectra is facilitated by computational methodologies such as modern density functional theory (DFT),[21−25] static exchange (STEX),[26] algebraic diagrammatic construction (ADC(2)),[27,28] and restricted active space self-consistent field (RASSCF).[29] The primary focus has therefore been centered on modeling individual molecules, effectively gas phase calculations, and one or more surrounding molecules. While this can often reproduce many features, particularly for inorganic-based systems,[25,29] there are clear implications for electronic structure in not accounting for the full structure (e.g., impact on energy levels, band gaps, molecular orbital distributions[30]) through intermolecular and long-range interactions/effects. The importance and strength of intermolecular hydrogen-bonding has, for example, been highlighted for simple carboxylic acids, where significant energy shifts were observed in both experimental and calculated NEXAFS on moving from monomers to dimers.[21] A combination of NEXAFS, XPS, and DFT calculations also revealed the interplay between core and valence level binding energy shifts in aqueous formic acid solutions at different pH-values.[24] Recent additions to the DFT code CASTEP[31] enable the prediction of core-level spectra from crystal structure information.[32−34] This development has

Received: July 13, 2014
Revised: September 23, 2014
Published: September 24, 2014

   dx.doi.org/10.1021/jp506983s | *J. Phys. Chem. B* 2014, 118, 12121−12129

significant relevance for the analysis of the organic solid state because CASTEP permits highly accurate modeling, taking the full three-dimensional crystal structure environment including all relevant intermolecular interactions into account. DFT codes such as CASTEP are increasingly used to predict and explain physical properties of organic solid state systems, such as electronic[35] and luminescent properties,[30,36] crystal polymorphism and stability,[37] and even nucleation pathways[38] and crystal structure.[39] The ability to use experimental core level spectra to interrogate the validity of such property predictions incisively, by direct reference to the molecular models used in the property calculations, constitutes an opportunity to facilitate further progress in this field.

In the following, we will show how CASTEP, XPS, and NEXAFS combined establish a protocol for investigating intermolecular interactions in organic molecular crystals with very high sensitivity. The α-polymorph of *para*-aminobenzoic acid (α-PABA, Figure 1), an intermediate for folic acid

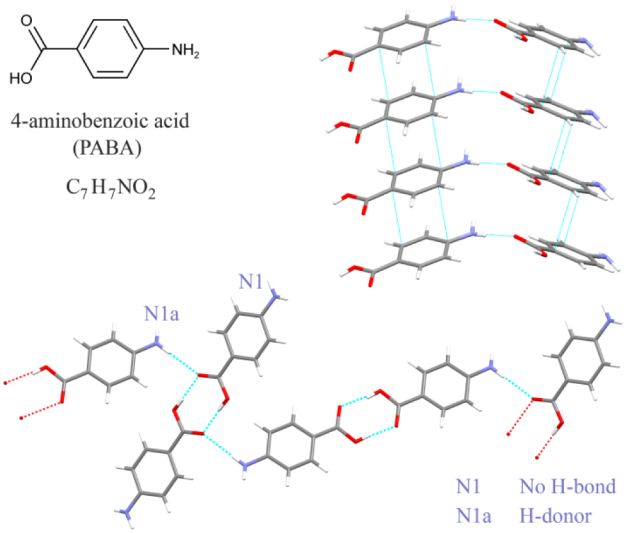

Figure 1. Structural motifs in the α-PABA crystal structure, illustrating dimers and intermolecular bonding as well as π stacking.

synthesis with pharmaceutical applications,[40,41] was chosen for our study. PABA contains both amine and carboxylic acid groups, providing spectroscopic contrast, and the crystal structure of α-PABA represents some of the most typical intermolecular interactions for organic systems,[42] exhibiting hydrogen-bonded carboxylic acid dimers, intermolecular N–H···O hydrogen-bonds that link the sets of dimers, and π–π stacking between offset aromatic rings.[43,44] It is therefore interesting to examine how these local interactions in the crystal environment are reflected in the core level spectra. As we will show below, after establishing accurate modeling of the solid state core level spectra by CASTEP, this can be achieved by comparison with CASTEP-predicted spectra for isolated PABA monomers.

EXPERIMENTAL AND COMPUTATIONAL DETAILS

Starting Materials. The α-form of 4-aminobenzoic acid (*para*-aminobenzoic acid, PABA) was obtained with >99% purity (Sigma-Aldrich, UK) and used as supplied. The α-form was confirmed by powder X-ray diffraction (PXRD, available as Supporting Information) through comparison with that simulated from the single crystal XRD structure[43] (some variation in intensities was observed with preferred orientation of the needle-like crystals). The PXRD pattern was collected using a Rigaku Miniflex instrument utilizing Cu K_α radiation (λ = 1.5406 Å), operating over 5–40° 2θ at 1.5° min^{-1} with a 0.03° step, 30 kV voltage, and 15 mA current.

X-ray Photoelectron Spectroscopy (XPS). XP spectra were recorded with a Kratos Axis Ultra instrument, employing a monochromatic Al K_α source (1486.69 eV), a hemispherical analyzer with a hybrid (electrostatic and magnetic) lens system, a charge neutralization system based on filament-generated, magnetically channeled low-energy electrons, and a delay line detector (DLD). Samples were fixed using double-sided tape. Experiments were performed while operating the X-ray source with a power of 180 W (15 kV and 12 mA), with the pressure below 10^{-8} mbar during analysis. The instrument was operated in CAE (constant analysis energy) mode, with a pass energy of 20 eV for high-resolution scans of the photoemission from individual core levels, with a calibrated intensity/energy response and transmission function.[45] High resolution spectra were measured within the spectral range of interest (ca. ± 20 eV around the core level emission peaks) with 0.1 eV steps and 500 ms dwell time per data point. Repeats were carried out to check for radiation damage.

Analysis of the data was carried out with CasaXPS software.[46] A Shirley background was used in all curve-fitting (minimizing χ^2)[4,46] along with a GL(30) line shape (70% Gaussian, 30% Lorentzian using the Gaussian/Lorentzian product form).[46] Samples were referenced to the lowest E_B photoemission C=C at 284.8 eV.[47] In the text, the atom of interest is indicated by being underlined. Repeatability of the peak positions was < ± 0.1 eV.

NEXAFS Spectroscopy. NEXAFS measurements were performed at the U7a beamline of the National Synchrotron Light Source (NSLS) at Brookhaven National Laboratory, NY. Partial electron yield (PEY) spectra for the C, N, and O K-edges were collected via a channeltron electron multiplier with the sample at the magic angle (54.7°) relative to the incident beam. An entrance grid bias of −50 V for C, −150 V for N, and −300 V for the O K-edge was used for PEY collection. Data for carbon were also collected at −150 V to show that the bias and therefore slight variation of information depth (increased surface sensitivity with more negative bias[48]) does not play a major role in the overall shape of the spectra in this case (spectra available as Supporting Information). A monochromator with a 600 l/mm grating was used for the C and N K-edges, providing energy resolution of 0.1 eV for C and ~0.15 eV for N and photon flux of ~2×10^{11} photons/s; and 1200 l/mm for the O K-edge with an energy resolution of ~0.15 eV and photon flux of ~1×10^{11} photons/s (comparable to the XPS Al K_α source[49]). After collection, the spectra were normalized by the simultaneously recorded drain current (total electron yield, TEY) from an in situ gold-coated, 90% transmission grid (I_0) placed in the incident X-ray beam to eliminate the effect of incident beam intensity fluctuations and beamline optics absorption features. The monochromator energy scale was calibrated using the 285.1 eV first π^* transition of an amorphous carbon grid for the C K-edge, 400.6 eV first π^* on a titanium nitride grid for N, and I_0 first minimum at 531.2 eV for O. Repeats were carried out to check for radiation damage.

Peak fitting and normalization was performed using the Athena software,[50,51] with arctan steps for the ionization potentials (IPs; edge steps) and Gaussian functions for the

dx.doi.org/10.1021/jp506983s | J. Phys. Chem. B 2014, 118, 12121–12129

peaks.[20,52] Modeling with Gaussian−Lorentzian lines is expected to be a valid method for determining the characteristic transition energies relating to π^* and σ^* orbitals.[20] At higher photon energies, in the extended X-ray absorption fine-structure (EXAFS) region, where the absorption spectra are mainly influenced by electron backscattering, the fitted peaks are merely a method for heuristic modeling of the spectral background, the fitted functions are therefore physically meaningless in this region, but we found their inclusion necessary to ensure reliable results in the spectral region of the electronic transitions to unoccupied bound states, i.e., just above and below the IPs. Generally good agreement of determined IP shifts with XPS-derived core level shifts, and good agreement with the sequences of Gaussian derived MO energies validate the methodology. More accurate interpretation can be obtained by DFT calculations of the whole spectra, as described in the next section.

DFT Methodology: CASTEP, WIEN2K, GAUSSIAN. A DFT strategy was utilized to predict core-level spectroscopy results *ab initio*. First the CASTEP code was used,[31] including recent additions to the code for the calculation of spectra.[32−34] The two key parameters to converge in the CASTEP DFT code are the basis set size (as defined by the value of the kinetic energy cutoff) and the sampling of *k*-points in reciprocal space. These parameters were converged according to a previously developed methodology[53] and the generalized gradient approximation (GGA) was used throughout.[54] The kinetic energy cutoff value was converged first. This was increased in intervals of 100 eV, and convergence was assessed against an actual predicted core-level spectrum (in this instance for one of the nitrogen atoms in the theoretical cell, the calculation being carried out in the ground electronic state). Upon changing the kinetic energy cutoff value from value 'X' to value 'Y', for each axis point on the energy axis (from −5.0 to 50 eV in intervals of 0.05 eV), the modulus of difference in predicted intensity value was found. These changes were then expressed as percentages relative to result 'X', and then averaged. When the average percentage change was lower than 15% (i.e., virtually no change could be seen "by eye") the result was considered to be converged. Ultimately, a kinetic energy cutoff value of 725 eV was chosen (Table 1).

Table 1. Convergence Systems and Final Chosen Parameters for the CASTEP Code (Used to Model Individual Atomic Core-Level Spectra)

cell details (single cell)	kinetic energy cutoff/eV	minimum *k*-point separation in reciprocal space
a = 18.63 Å, b = 3.84 Å, c =25.45 Å, $\alpha = \gamma = 90°$, β = 133.27° ($P2_1/c$)[44]	725	0.032 Å^{-1} (revised to 0.064 Å^{-1} when computational memory considerations forced this)

An analogous process was carried out to converge the *k*-point grid in reciprocal space. The *k*-point grid used the Monkhorst−Pack form.[55] As the single cell of α-PABA is not cubic, a grid was chosen to reflect this, such that the *k*-point spacing in each dimension was approximately similar. In terms of the actual convergence process, the number of *k*-points in each dimension was doubled until convergence was achieved.

For the convergence experiments, cell symmetry had been applied such that the crystal structure was in the form $P2_1/c$ (a = 18.63 Å, b = 3.84 Å, c = 25.45 Å, $\alpha = \gamma = 90°$, β = 133.27°).[44] The core-hole was converged against cell size in order to utilize fractional core-holes. Examining the lattice parameters detailed above, a and c are large, and it was therefore postulated that b was the key dimension to expand as part of the convergence process. Therefore, a 1 × 2 × 1 supercell was generated, and a predicted nitrogen K-edge was found for the same "symmetry" of nitrogen atom as in the other convergence experiments. The predicted spectrum was then compared between the different cell sizes (in both instances with a 0.5 electron core-hole in place). Again it was observed there was little difference between the predicted spectra, so a 1 × 2 × 1 supercell of this form was considered suitable. For practical considerations (computer memory), the *k*-point grid sampling density had to be reduced in some instances (this is also as described in Table 1).

The all-electron code, WIEN2K, was used to predict the onset energy shifts *ab initio* (for example, between a carbonyl carbon atom and an aromatic carbon atom).[56] Again, it was necessary to carry out a convergence process to properly select parameters for the WIEN2K code. Given that WIEN2K is also a linearized augmented plane wave (LAPW) code like CASTEP, these were the basis set size, and the density of *k*-points in reciprocal space. In WIEN2K, the former is defined by the RK_{MAX} value. These parameters were converged such that predicted energy separations (for example between the two crystallographically nonequivalent nitrogen atoms in a PABA unit cell) were accurate to ±0.001 eV. The splittings were determined *ab initio* and are compared to the values we obtained experimentally by XPS.

In Table 5, the various shifts are averaged for each class of functional group for comparison with the experimental XPS results (there are a total of 14 crystallographically different carbon environments in the PABA cell, 4 oxygen environments, and 2 nitrogen environments due to the two asymmetric molecules in the unit cell). *Ab initio* splittings were determined in each instance, as were CASTEP-predicted core-level NEXAFS spectra for the individual atomic positions. For each position therefore, the spectrum was rigid-shifted by the required amount in the energy axis, and then an energy-dependent lifetime broadening was applied.[57] Following this, the spectra for each atomic species were averaged. For the crystallographically independent molecules, the shift between comparable atoms is below experimentally achievable resolution, for example, the energetic separation between the two crystallographically inequivalent nitrogen atoms in the unit cell was found to be 0.024 eV.

For the nitrogen K-edge, predicted spectra obtained with atomic positions from the published X-ray diffraction (XRD) single crystal structure[44] did not adequately reproduce the shape of the experimental spectrum. As XRD probes electron density rather than the position of nuclei, the refined hydrogen position in the crystal structure is systematically shifted slightly closer to the atom it is covalently bonded to, shortening the X−H bond length by ∼0.1 Å relative to the hydrogen position from neutron diffraction.[58−61] Therefore, a geometry optimization of the crystal structure was performed. The geometry optimization calculation was performed using CASTEP, starting from the crystal structure,[44] and employing the Tkatchenko−Scheffler correction to account for dispersive forces.[62] The exit criteria for geometry optimization (using BFGS methodology[63−65]) were set such that for the structure to be considered minimized as part of an iterative process the energy change per atom was less than 2.0×10^{-5}, the maximum force change 0.05 eVÅ^{-1}, the maximum stress change 0.1 GPa

dx.doi.org/10.1021/jp506983s | J. Phys. Chem. B 2014, 118, 12121−12129

and the maximum displacement of atoms 0.002 Å. The overall space group of the system was not allowed to change during the geometry optimization process, but the lattice dimensions did alter. The results of the optimization showed that an increase in N−H bond length by ∼0.1 Å relative to the value in the published single crystal structure achieved satisfactory agreement with the experimental nitrogen K-edge NEXAFS.

For the carbon, nitrogen, and oxygen K-edge monomer calculations, a single molecule of PABA was taken from the α-polymorph crystal structure,[44] without further structural minimization, and isolated in a 10 Å cubic box. The calculation was then repeated for a 15 Å box. There were no significant changes in the predicted spectrum, so this size was considered sufficiently large to isolate the PABA molecule and approximately simulate the gas phase monomer. A 0.5 electron core-hole was used for the data presented. Again, as with the crystal form, the structure was subject to geometry optimization as described above. In the figures below, for both the monomer and the crystal, the nitrogen K-edges were calculated from the optimized crystal structure, while the other edges were calculated from the published crystal structure.[44] As for the crystal, the actual predicted shifts for each specific position (WIEN2K convergence experiments accurate to ±0.01) for the monomer were combined with the CASTEP spectra, with the application of appropriate broadening.

An α-PABA monomer was also optimized with the B3LYP functional and 6-31G* basis set in Gaussian 09[66] to visualize[67] molecular orbitals for the ground state.

RESULTS AND DISCUSSION

Crystal. Despite being a small organic molecule, PABA has a significant variety of atomic, and more importantly chemical, moieties (C═C, C−N, COOH for carbon, O═C−OH, O═C−OH for oxygen, NH_2 for nitrogen, Figure 2). The atomic

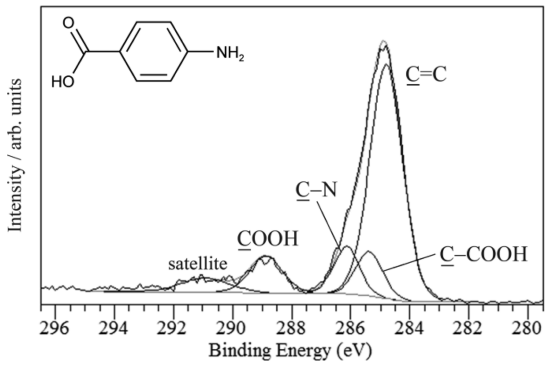

Figure 2. Experimental C 1s XPS of α-PABA and the fitted component peaks, showing the shifts in binding energy (IP) for different chemical species.

chemical-state specificity in XPS is evidenced through the clear chemical shifts in core level 1s binding energies (IPs) for the different chemical environments, such as +1.3 eV for C−N and +4.0 eV for COOH carbons relative to the unsubstituted aromatic ring C═C atoms at 284.8 eV in the C 1s photoemission (Figure 2). NEXAFS experimental spectra for the crystalline (solid) α-PABA reveal significant fine structure around the carbon, nitrogen, and oxygen K-edges (Figure 3, 4, and 5), with sharp pre-edge 1s → π^* resonances followed by broader features representing 1s → σ^* contributions above each edge. The distinct IPs for the different chemical moieties

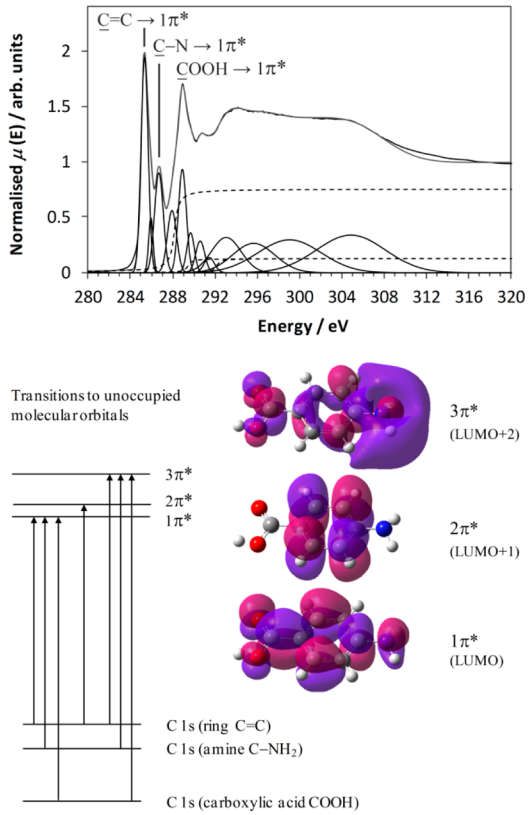

Figure 3. Experimental carbon K-edge NEXAFS of α-PABA and a model of the spectrum obtained by fitting Gaussian (peak) and arctan step (edge IP) functions, and schematic of transitions from carbon core 1s levels to the three lowest unoccupied MOs (LUMOs) for PABA based on XPS/NEXAFS (ground-state MO representations).

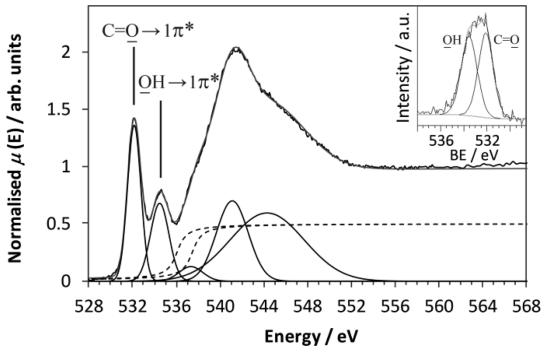

Figure 4. Experimental oxygen K-edge NEXAFS of α-PABA and a model of the spectrum obtained by fitting Gaussians and arctan step functions, along with the O 1s XPS in the inset.

are also reflected by the inflection points of the edge step functions in NEXAFS. Additionally, there are characteristic 1s → π^* transitions for each chemical species (as seen for the carbon moieties in Figure 3).

The two chemically distinct oxygen atoms of the carboxylic acid group also lead to different chemical shifts in XPS, with the O 1s carbonyl O═C−OH photoemission peak at 532.1 eV and the hydroxyl O═C−OH at 533.5 eV (Figure 4 inset). Separations in energy are also revealed in the pre-edge region of the NEXAFS spectra since resonances result from electron promotion from the core levels (Figure 3), and this is evident in the energy shifts between the 1s → 1π^* peaks for the different carbon (Figure 3) and oxygen (Figure 4) species. A view of the

dx.doi.org/10.1021/jp506983s | J. Phys. Chem. B 2014, 118, 12121−12129

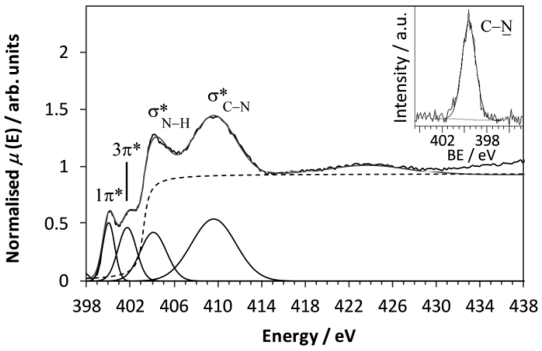

Figure 5. Experimental nitrogen K-edge NEXAFS of α-PABA and a model of the spectrum obtained by fitting Gaussians and an arctan step function, along with the N 1s XPS in the inset.

energy levels and molecular orbitals (MOs) of PABA (Figure 3) shows that additional NEXAFS intensity may arise from 1s → 2π* (carbon only) and 1s → 3π* contributions toward higher energy (Tables 2, 3, and 4). This results in several additional pre-edge features for carbon (Table 2), including C=C → 3π* and C–N → 3π* transitions leading to visible shoulders on either side of the COOH → 1π* peak (Figure 3).

While there are several carbon and oxygen chemical environments within PABA, there is only one type of nitrogen (aromatic NH_2), resulting in a single N 1s signal at 399.6 eV for the nitrogen functional group, the primary aromatic amine NH_2 (Figure 5 inset). The nitrogen K-edge spectrum (Figure 5) is therefore a very sensitive and rather unequivocal probe of local electronic structure, with two pre-edge resonances arising from promotion from the N 1s into 1π* and 3π* unoccupied MOs, respectively. Note that the N 1s → 2π* transitions are not expected to be significant as the 2π* MO has no density at the nitrogen absorber (Figure 3). While π* resonances show chemical and electronic specificity, the position of the σ* resonances relative to the IP (the so-called "term value" δ) can be related to the intramolecular distance between absorber atom and its covalently bonded neighbor, providing a particularly sensitive measure of bond length.[20,68] For α-PABA, the σ^*_{C-N} resonance occurs at a higher energy relative to the IP (δ = 6.3 eV) than for the structurally related aniline (δ = 2.3 eV), reflecting the influence of the shortened C–N bond length for PABA (1.38 Å[43,44] vs 1.43 Å for aniline[69]) and the influence of subtleties in bonding on the NEXAFS spectra.

An *ab initio* prediction of the NEXAFS of molecules in the α-PABA crystal structure was carried out with CASTEP, using the core level shifts from WIEN2K for the different chemical environments as described above. The predicted core level shifts for the crystal structure match experiment quite well (Table 5), considering the complexity of the electronic, chemical, and structural influences on the excitation and relaxation in the photoemission process and treatment of the core hole and Coulomb potentials to be taken into account when trying to predict these splitting, such that accuracy of ca. 0.3 eV relative to experiment is currently optimal in all but the most computationally expensive methods.[70−73] The calculated NEXAFS thus takes the molecular conformation, the three-dimensional coordination and the resulting intermolecular interactions (Figure 1) into account for each functional group. Using atomic positions from the published α-PABA crystal structure,[44] all pre-edge π* features for carbon were successfully reproduced by the calculation, and so was the overall shape of the post-edge structure (Figure 6). Despite the multiple types of carbon moieties present in PABA, transitions arising from the core 1s level to the unoccupied 1π* MO are clearly visible

Table 2. C K-edge NEXAFS Resonances and Assignments Based on Potential Transitions for α-PABA[a]

NEXAFS C K-edge	transition/eV
IP (C=C)	288.10
IP (C–N)	289.40
IP (COOH)	292.10
C 1s (C=C) → 1π*	285.28
C 1s (C=C–COOH) → 1π*/C 1s (C=C) → 2π*	285.87
C 1s (C–N) → 1π*	286.63
C 1s (C=C) → 3π*	287.87
C 1s (COOH) → 1π*	288.85
C 1s (C–N) → 3π*	289.63
C 1s (C=C) → 4π*	290.54
C 1s (COOH) → 3π*	291.40

[a]The values were obtained from the fitted model in Fig. 3.

Table 3. O K-Edge NEXAFS Resonances and Assignments Based on Potential Transitions for α-PABA[a]

NEXAFS O K-edge	transition/eV
IP (O=C–OH)	535.70
IP (O=C–OH)	537.10
O 1s (O=C–OH) → 1π*	532.08
O 1s (O=C–OH) → 1π*/O 1s (O=C–OH) → 3π*	534.41
O 1s (O=C–OH) → 3π*	537.26

[a]The values were obtained from the fitted model in Figure 4.

Table 4. N K-edge NEXAFS Resonances and Assignments Based on Potential Transitions for α-PABA[a]

NEXAFS N K-edge	transition/eV
IP (aromatic NH_2)	403.30
N 1s → 1π*	400.00
N 1s → 3π*	401.70
N 1s → σ^*_{N-H}	404.09
N 1s → σ^*_{C-N}	409.61
δ_{C-N} (σ^*_{C-N} − IP)	6.31

[a]The values were obtained from the fitted model in Figure 5.

Table 5. Experimental XPS and Theoretical WIEN2K Core Level Shifts for Carbon and Oxygen in the α-PABA Crystal Structure along with That Calculated for an Isolated Monomer

	core level 1s binding energy/eV			
C 1s	C=C	C–COOH	C–N	COOH
exp. crystal	0[a]	+0.45	+1.30	+4.00
crystal	0[a]	+0.44	+1.75	+3.71
monomer	0[a]	+0.42	+1.74	+2.75
O 1s		O=C–OH		O=C–OH
exp. crystal		0[a]		+1.40
crystal		0[a]		+1.19
monomer		0[a]		+2.23

[a]Reference photoemission line.

dx.doi.org/10.1021/jp506983s | J. Phys. Chem. B 2014, 118, 12121−12129

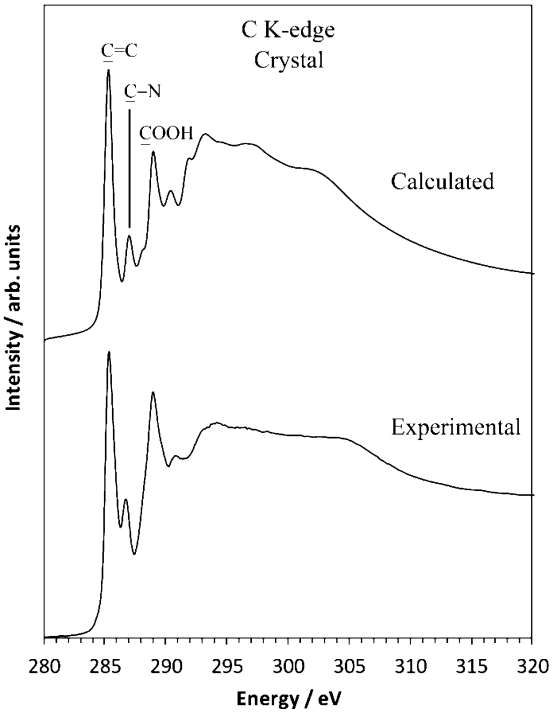

Figure 6. Comparison of edge-step normalized theoretical and experimental carbon K-edge NEXAFS for crystalline α-PABA, with the 1s → 1π* transitions indicated.

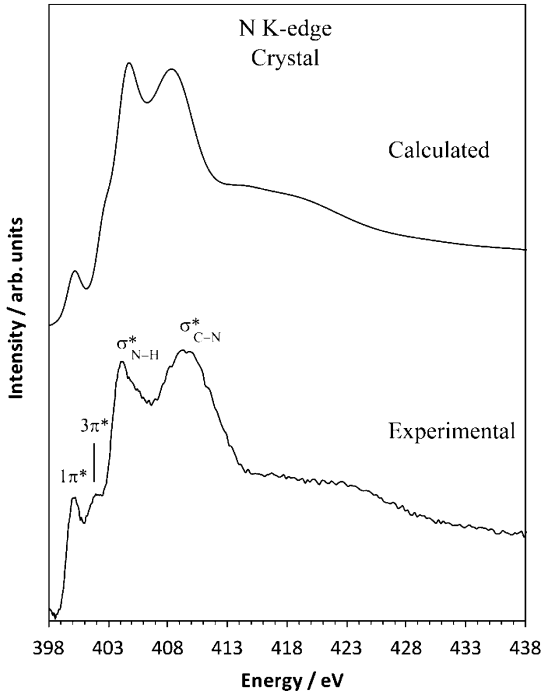

Figure 7. Comparison of calculated and experimental edge-step normalized nitrogen K-edge NEXAFS for crystalline α-PABA.

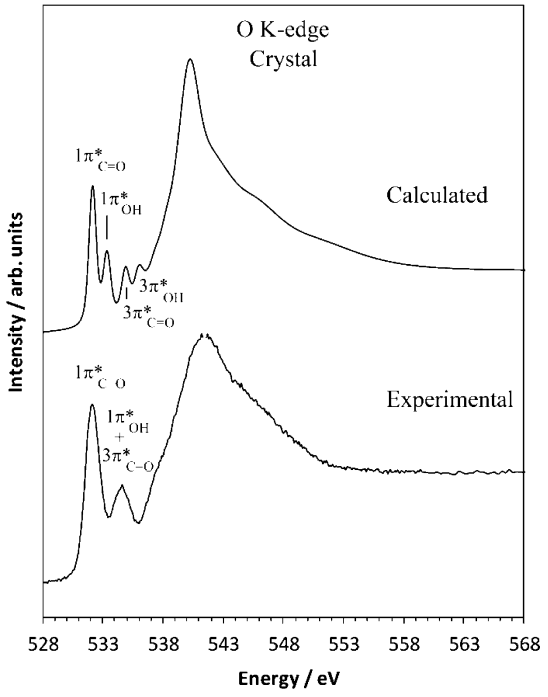

Figure 8. Comparison of theoretical and experimental edge-step normalized oxygen K-edge NEXAFS for crystalline α-PABA, with the 1s → 1π* and 1s → 3π* transitions indicated.

for the C=C, C–N, and COOH absorbers (Figure 6), alongside peaks arising from the higher C=C π* resonances at ca. 288 and 290.5 eV (either side of the COOH 1π*) and the COOH → 3π* at 291.5 eV. All corresponded well with both the energy and relative intensity of the experimentally observed resonances.

The sensitivity of electronic structure to even minor variations in the local structure around the X-ray absorber is clearly illustrated through the calculation for nitrogen in the crystal structure, which required further refinement of the published crystal structure (as described in the Experimental and Computational Details section) to achieve a good match with experiment (Figure 7). The refinement lengthened the N–H bonds by ~0.1 Å relative to the published XRD crystal structure,[44] in line with the results of more accurate neutron diffraction analysis,[61] notably shifting the σ^*_{N-H} peak to lower energy.

Prediction of the oxygen K-edge from the published crystal structure[44] produces a good match with experiment in the post-edge region, while there appear to be additional peaks in the pre-edge region (Figure 8). The shift between the 1s → 1π* peaks is often dominated by contributions from the 1s core level chemical shifts (initial-state),[20] and for the predicted spectrum of the crystal the splitting between the π* resonances for the C=O and OH oxygen species is determined by the core level shift (1.19 eV from WIEN2K, Table 5). This is significantly smaller than the 2.33 eV offset between the two 1π* resonances found with NEXAFS experimentally (Figure 8, Table 3).[21,22,74] The 1s → π* transitions are not only sensitive to the localized electron density probed with photoemission from 1s core levels in XPS, but also to orbital correlation with neighboring atoms and the differing effects of core hole interactions and relaxation,[20] and this appears to be more significant for oxygen than carbon for different functional groups. Adjusting the calculated oxygen K-edge NEXAFS to the experimentally observed 1s → 1π* shift would move the second and fourth resonances ($1\pi^*_{OH}$ and $3\pi^*_{OH}$, respectively) to higher energy by ca. 1 eV, leading to superposition of the second and third resonances ($1\pi^*_{OH}$ and $3\pi^*_{C=O}$), and this would achieve good agreement between experiment and calculation.

dx.doi.org/10.1021/jp506983s | J. Phys. Chem. B 2014, 118, 12121–12129

Monomer. Having established that we can predict the solid state NEXAFS with high accuracy, we can now examine the expected differences to spectra of an isolated PABA monomer. This analysis reveals the effects of the surrounding environment and local interactions on the NEXAFS and electronic structure. Figure 9 compares the CASTEP-calculated α-PABA NEXAFS spectra of carbon, nitrogen, and oxygen to those predicted for monomers.

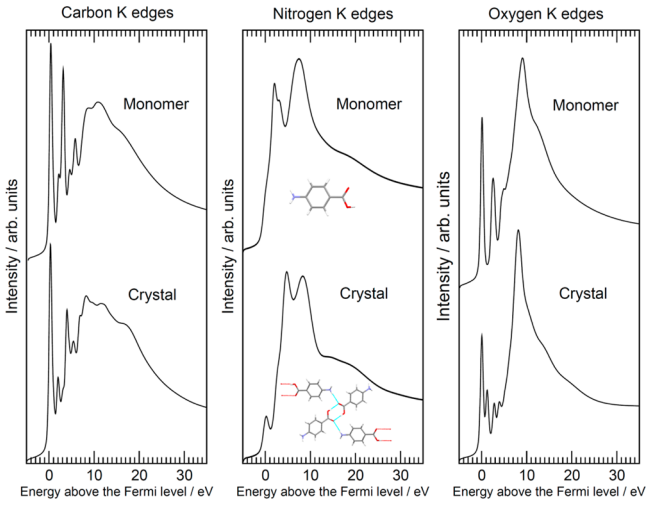

Figure 9. Comparison of predicted carbon, nitrogen, and oxygen K-edges for the α-crystal and an isolated monomer of PABA (monomer spectra aligned to crystal results; optimized structure for nitrogen), highlighting the influence of the three-dimensional environment and intermolecular interactions, particularly the H-bonded dimer, in the α-crystal structure.

On moving from the extended crystal structure (Figure 1) to an isolated monomer, the local three-dimensional environment is changed and the intermolecular interactions are lost, and there is significant impact on the atoms directly involved in these interactions. One of the most notable differences between the crystal and monomer affecting the carbon and oxygen atoms is the loss of the hydrogen-bonded carboxylic acid dimer (Figure 9), leading to the two oxygen environments (C═O and OH) becoming increasingly different in electronic character. This leads to a larger O 1s core level chemical shift between the two oxygen atoms for the monomer (approximately an additional 1 eV, Table 5), as well as to impact on the properties of the carbon atom within the carboxylic acid group (COOH), with a C 1s core level binding energy lowered by 1 eV for the monomer. This is readily explained by the fact that dimer formation in the crystal structure withdraws electron density from carbon, causing a higher C 1s binding energy. There is also a widening of the separation between the oxygen K-edge pre-edge resonances arising from transitions to the π^* orbitals (Figure 9, right).[21] Similarly, the energy and intensity variation for the COOH carbon 1s → $1\pi^*$ resonance (third sharp peak), as well as the 1s → $3\pi^*$ for COOH (fourth sharp peak), is a major factor in altering the overall carbon K-edge spectra between the monomer and crystal (Figure 9, left), with a shift to lower energy following the decrease in core level binding energy with loss of the dimer.

For nitrogen, the loss of NHO hydrogen-bonding in the monomer (Figure 9) leads to slight variation in the core levels[7] through alteration of the electronic character at nitrogen, while loss of the COOH dimers also indirectly affects the nitrogen through the conjugation of electron density across the aromatic ring. The shifts between pre-edge resonances for nitrogen (Figure 9, center) are linked to changes in electronic structure as they primarily arise from alterations in the unoccupied π^* orbitals rather than the core level since transitions originate from one type of N 1s level. At an intramolecular level, the N−H and C−N bond lengths are comparable for both the monomer and optimized crystal (1.01/1.02 Å and 1.371/1.376 Å respectively), showing that the resonances are also influenced by hydrogen-bonding interactions and likely also weaker non-covalent interactions. The local geometry of the amine group changes from bent, quasi-pyramidal in the crystal structure to planar in the monomer (ca. 22° and 3° angle between the amine group and plane of aromatic ring respectively), which may also slightly affect the interaction and stabilization of the more diffuse unoccupied MOs. The observed spectral changes are interdependent, influenced by hydrogen-bonding, the three-dimensional geometrical arrangement in the crystal structure, and the $\pi-\pi$ interactions between the molecules. The clear variation between the monomer and crystal nitrogen K-edges poignantly illustrates the strength of the effect of the local environment and interactions (or lack thereof) on NEXAFS spectra (Figure 9, center).

CONCLUSIONS

Analysis of the substituted benzoic acid derivative PABA with both XPS and NEXAFS provides the chemical shifts for photoemission from different chemical environments and transition energies to unoccupied molecular orbitals. Prediction of the NEXAFS spectra through CASTEP allows the local interactions to be elucidated through use of crystal structure data. The agreement between experiment and theory is strong for the carbon, nitrogen, and oxygen K-edges. The decisive influence of small bond length variations was demonstrated for nitrogen and the importance of relatively weak energetic contributions of interactions such as H-bonding is reflected by the reproduction of the overall shape of the spectra. Moreover, use of the CASTEP code reveals the important influence of intermolecular interactions in the solid state through comparison of predictions for an isolated monomer and the crystal structure. This highlights the sensitivity of NEXAFS for probing interactions in the organic solid state, which permits validation of the predictions by CASTEP and other DFT modeling methods, taking the full three-dimensional crystal structure environment with all intermolecular interactions into account. It is probably reasonable to expect that the ability to use experimental core level spectra to validate computational predictions of physical properties can inform future development of even more accurate computational methods for solid state modeling. In the Introduction we already mentioned examples such as the prediction of electronic and luminescent properties,[30,35,36] polymorph stability, crystalline state, and nucleation species,[37−39] but this capability of NEXAFS is applicable in other fields and highlights a potential for further refinement of the relationships between DFT, experimental core level spectroscopy, and crystallography.

ASSOCIATED CONTENT

Supporting Information

Powder X-ray diffraction pattern for α-PABA and carbon K-edge NEXAFS measured at −50 and −150 V bias. This material is available free of charge via the Internet at http://pubs.acs.org.

AUTHOR INFORMATION

Corresponding Author

*E-mail: s.schroeder@manchester.ac.uk.

Notes

The authors declare no competing financial interest.

ACKNOWLEDGMENTS

This work made use of the facilities of N8 HPC provided and funded by the N8 consortium and EPSRC (Grant No. EP/K000225/1). The Centre is coordinated by the Universities of Leeds and Manchester. The authors would also like to acknowledge the usage of the ARC1 computing facility at the University of Leeds, and the usage of Hartree Centre resources for this work. The STFC Hartree Centre is a research collaboration funded by the UK's investment in e-Infrastructure. CRS would like to acknowledge the support of the High Performance Computing (HPC) team at the University of Leeds, for their design of the advanced research computing 1 (ARC1) facility, and assistance in code compilation and optimization. Use of the National Synchrotron Light Source, Brookhaven National Laboratory, was supported by the U.S. Department of Energy, Office of Science, Office of Basic Energy Sciences, under Contract No. DE-AC02-98CH10886. We gratefully acknowledge support for JSS, SLMS, CRS, and AJS through EPSRC Critical Mass Grants (EP/I013563/1 and EP/I014446/1). Commercial names mentioned in this manuscript are for illustrative purposes and do not represent an endorsement by the National Institute of Standards and Technology.

REFERENCES

(1) *Pharmaceutical Salts and Co-crystals*, 1st ed.; The Royal Society of Chemistry: Cambridge, 2012.

(2) *Handbook of Pharmaceutical Excipients*, 6th ed.; Pharmaceutical Press: London and Chicago, 2009.

(3) Schultheiss, N.; Newman, A. Pharmaceutical Cocrystals and Their Physicochemical Properties. *Cryst. Growth Des.* **2009**, *95*, 499−516.

(4) Briggs, D.; Seah, M. P.; Sherwood, P. M. A. In *Practical Surface Analysis: Auger and X-ray Photoelectron Spectroscopy*, 2nd ed.; Briggs, D.; Seah, M. P., Eds. John Wiley & Sons: Chichester, 1990; Vol. *1*.

(5) Stöhr, J.; Sette, F.; Johnson, A. L. Near-Edge X-ray-Absorption Fine-Structure Studies of Chemisorbed Hydrocarbons: Bond Lengths with a Ruler. *Phys. Rev. Lett.* **1984**, *53*, 1684−1687.

(6) Bisti, F.; Stroppa, A.; Picozzi, S.; Donarelli, M.; Picozzi, S.; Coreno, M. The Electronic Structure of Gas Phase Croconic Acid Compared to the Condensed Phase: More Insight into the Hydrogen Bond Interaction. *J. Chem. Phys.* **2013**, *138*, 014308−1−014308−4.

(7) Stevens, J. S.; Byard, S. J.; Seaton, C. C.; Sadiq, G.; Davey, R. J.; Schroeder, S. L. M. Proton Transfer and Hydrogen Bonding in the Organic Solid State: A Combined XRD/XPS/ssNMR Study of 17 Organic Acid-Base Complexes. *Phys. Chem. Chem. Phys.* **2014**, *16*, 1150−1160.

(8) Stevens, J. S.; Byard, S. J.; Seaton, C. C.; Sadiq, G.; Davey, R. J.; Schroeder, S. L. M. Crystallography Aided by Atomic Core-Level Binding Energies: Proton Transfer Versus Hydrogen Bonding in Organic Crystal Structures. *Angew. Chem., Int. Ed.* **2011**, *50*, 9916−9918.

(9) Stevens, J. S.; Byard, S. J.; Schroeder, S. L. M. Salt or Co-Crystal? Determination of Protonation State by X-ray Photoelectron Spectroscopy (XPS). *J. Pharm. Sci.* **2010**, *99*, 4453−4457.

(10) Stevens, J. S.; Byard, S. J.; Muryn, C. A.; Schroeder, S. L. M. Identification of Protonation State by XPS, Solid-State NMR, and DFT: Characterization of the Nature of a New Theophylline Complex by Experimental and Computational Methods. *J. Phys. Chem. B* **2010**, *114*, 13961−13969.

(11) O'Shea, J. N.; Schnadt, J.; Bruhwiler, P. A.; Hillesheimer, H.; Martensson, N.; Patthey, L.; Krempasky, J.; Wang, C.; Luo, Y.; Agren, H. Hydrogen-Bond Induced Surface Core-Level Shift in Isonicotinic Acid. *J. Phys. Chem. B* **2001**, *105*, 1917−1920.

(12) Tu, G.; Tu, Y.; Vahtras, O.; Agren, H. Core Electron Chemical Shifts of Hydrogen-Bonded Structures. *Chem. Phys. Lett.* **2009**, *468*, 294−298.

(13) Ito, E.; Oji, H.; Araki, T.; Oichi, K.; Ishii, H.; Ouchi, Y.; Ohta, T.; Kosugi, N.; Maruyama, Y.; Naito, T.; et al. Soft X-ray Absorption and X-ray Photoelectron Spectroscopic Study of Tautomerism in Intramolecular Hydrogen Bonds of *N*-Salicylideneaniline Derivatives. *J. Am. Chem. Soc.* **1997**, *119*, 6336−6344.

(14) Ramasse, Q. M.; Seabourne, C. R.; Kepaptsoglou, D.-M.; Zan, R.; Bangert, U.; Scott, A. J. Probing the Bonding and Electronic Structure of Single Atom Dopants in Graphene with Electron Energy Loss Spectroscopy. *Nano Lett.* **2013**, *13*, 4989−4995.

(15) Aplincourt, P.; Bureau, C.; Anthoine, J.-L.; Chong, D. P. Accurate Density Functional Calculations of Core Electron Binding Energies on Hydrogen-Bonded Systems. *J. Phys. Chem. A* **2001**, *105*, 7364−7370.

(16) Garcia-Gil, S.; Arnau, A.; Garcia-Lekue, A. Exploring Large O 1s and N 1s Core Level Shifts Due to Intermolecular Hydrogen Bond Formation in Organic Molecules. *Surf. Sci.* **2013**, *613*, 102−107.

(17) Lange, K. M.; Könnecke, R.; Soldatov, M.; Golnak, R.; Rubensson, J.-E.; Soldatov, A.; Aziz, E. F. On the Origin of the Hydrogen-Bond-Network Nature of Water: X-ray Absorption and Emission Spectra of Water−Acetonitrile Mixtures. *Angew. Chem., Int. Ed.* **2011**, *50*, 10621−10625.

(18) Petit, T.; Lange, K. M.; Conrad, G.; Yamamoto, K.; Schwanke, C.; Hodeck, K. F.; Dantz, M.; Brandenburg, T.; Suljoti, E.; Aziz, E. F. Probing Ion-Specific Effects on Aqueous Acetate Solutions: Ion Pairing Versus Water Structure Modifications. *Struct. Dynam.* **2014**, *1*, 034901−1−03901−8.

(19) Stevens, J. S.; Byard, S. J.; Schroeder, S. L. M. Characterization of Proton Transfer in Co-crystals by X-ray Photoelectron Spectroscopy (XPS). *Cryst. Growth Des.* **2010**, *10*, 1435−1442.

(20) Stöhr, J. *NEXAFS Spectroscopy*. 2nd ed.; Springer-Verlag: Berlin, 1992.

(21) Tabayashi, K.; Takahashi, O.; Namatame, H.; Taniguchi, M. Substituent R-Effects on the Core-Electron Excitation Spectra of Hydrogen-Bonded Carboxylic-Acid (R-COOH) Clusters: Comparison between Acetic-Acid and Formic-Acid Clusters. *Chem. Phys. Lett.* **2012**, *557*, 1−9.

(22) Zhang, W.; Nefedov, A.; Naboka, M.; Cao, L.; Woll, C. Molecular Orientation of Terephthalic Acid Assembly on Epitaxial Graphene: NEXAFS and XPS Study. *Phys. Chem. Chem. Phys.* **2012**, *14*, 10125−10131.

(23) Lopez, A.; Bitzer, T.; Heller, T.; Richardson, N. V. Functional Group Selectivity in Adsorption of 4-Aminobenzoic Acid on Clean and Na Modified Si(100)-2 × 1 Surfaces. *Surf. Sci.* **2001**, *480*, 65−72.

(24) Brown, M. A.; Vila, F.; Sterrer, M.; Thürmer, S.; Winter, B.; Ammann, M.; Rehr, J. J.; van Bokhoven, J. A. Electronic Structures of Formic Acid (HCOOH) and Formate ($HCOO^-$) in Aqueous Solutions. *J. Phys. Chem. Lett.* **2012**, *3*, 1754−1759.

(25) Xiao, J.; Golnak, R.; Atak, K.; Pflüger, M.; Pohl, M.; Suljoti, E.; Winter, B.; Aziz, E. F. Assistance of the Iron Porphyrin Ligands to the Binding Interaction Between the Fe Center and Small Molecules in Solution. *J. Phys. Chem. B* **2014**, *118*, 9371−9377.

(26) Plashkevych, O.; Yang, L.; Vahtras, O.; Ågren, H.; Petterson, L. G. M. Substituted Benzenes as Building Blocks in Near-Edge X-ray Absorption Spectra. *Chem. Phys.* **1997**, *222*, 125−137.

(27) Schirmer, J. Beyond the Random-Phase Approximation: A New Approximation Scheme for the Polarization Propagator. *Phys. Rev. A* **1982**, *26*, 2395−2416.

(28) Bâldea, I.; Schimmelpfennig, B.; Plaschke, M.; Rothe, J.; Schirmer, J.; Trofimov, A. B.; Fanghänel, T. C 1s Near Edge X-ray Absorption Fine Structure (NEXAFS) of Substituted Benzoic Acids −

A Theoretical and Experimental Study. *J. Electron Spectrosc. Relat. Phenom.* **2007**, *154*, 109−118.
(29) Bokarev, S. I.; Dantz, M.; Suljoti, E.; Kühn, O.; Aziz, E. F. State-Dependent Electron Delocalization Dynamics at the Solute-Solvent Interface: Soft-X-ray Absorption Spectroscopy and *Ab Initio* Calculations. *Phys. Rev. Lett.* **2013**, *111*, 083002−1−083002−5.
(30) Yan, D.; Bučar, D.-K.; Delori, A.; Patel, B.; Lloyd, G. O.; Jones, W.; Duan, X. Ultrasound-Assisted Construction of Halogen-Bonded Nanosized Cocrystals That Exhibit Thermosensitive Luminescence. *Chem.—Eur. J.* **2013**, *19*, 8213−8219.
(31) Clark, S. J.; Segall, M. D.; Pickard, C. J.; Hasnip, P. J.; Probert, M. I. J.; Refson, K.; Payne, M. C. First Principles Methods Using CASTEP. *Z. Kristallogr.: Cryst. Mater.* **2005**, *220*, 567−570.
(32) Pickard, C. J. *Ab Initio Electron Energy Loss Spectroscopy*; University of Cambridge: Cambridge, U.K., 2007.
(33) Gao, S.-P.; Pickard, C. J.; Payne, M. C.; Zhu, J.; Yuan, J. Theory of Core−Hole Effects in 1s Core-Level Spectroscopy of the First-Row Elements. *Phys. Rev. B: Condens. Matter Mater. Phys.* **2008**, *77*, 115122−1−115122−7.
(34) Gao, S.-P.; Chris, J. P.; Alexander, P.; Victor, M. Core-Level Spectroscopy Calculation and the Plane Wave Pseudopotential Method. *J. Phys.: Condens. Matter* **2009**, *21*, 104203−1−104203−12.
(35) Salzner, U. Electronic Structure of Conducting Organic Polymers: Insights from Time-Dependent Density Functional Theory. *Wiley Interdisciplinary Reviews: Computational Molecular Science* **2014**, DOI: 10.1002/wcms.1194.
(36) Yan, D.; Fan, G.; Guan, Y.; Meng, Q.; Li, C.; Wang, J. Tuning Solid-State Blue and Red Luminescence by the Formation of Solvate Crystals. *Phys. Chem. Chem. Phys.* **2013**, *15*, 19845−19852.
(37) Ectors, P.; Ectors, D.; Zahn, D. Structure and Interactions in Benzamide Molecular Crystals. *Mol. Simul.* **2014**, *39*, 1079−1083.
(38) Anwar, J.; Zahn, D. Uncovering Molecular Processes in Crystal Nucleation and Growth by Using Molecular Simulation. *Angew. Chem., Int. Ed.* **2013**, *50*, 1996−2013.
(39) Price, S. L. Predicting Crystal Structures of Organic Compounds. *Chem. Soc. Rev.* **2014**, *43*, 2098−2111.
(40) Wagner, A. F.; Folkers, K. *Vitamins and Coenzymes*; Interscience Publishers: New York, 1964.
(41) Staunton, E.; Todd, W. R.; Mason, H. S.; Bruggen, J. T. V. *Textbook of Biochemistry*; The MacMillan Company: New York, 1967.
(42) Allen, F. H. The Cambridge Structural Database: A Quarter of a Million Crystal Structures and Rising. *Acta Crystallogr., Sect. B: Struct. Sci.* **2002**, *B58*, 380−338.
(43) Lai, T. F.; Marsh, R. E. The Crystal Structure of P-Aminobenzoic Acid. *Acta Crystallogr.* **1967**, *22*, 885−893.
(44) Athimoolam, S.; Natarajan, S. 4-Carboxyanilinium (2R,3R)-Tartrate and a Redetermination of the α-Polymorph of 4-Aminobenzoic Acid. *Acta Crystallogr., Sect. C: Cryst. Struct. Commun.* **2007**, *63*, o514−o517.
(45) Stevens, J. S.; Schroeder, S. L. M. Quantitative Analysis of Saccharides by X-ray Photoelectron Spectroscopy. *Surf. Interface Anal.* **2009**, *41*, 453−462.
(46) Fairley, N.; Carrick, A. *The Casa Cookbook - Part 1: Recipes for XPS Data Processing*; Acolyte Science: Knutsford, Cheshire, U.K., 2005.
(47) Beamson, G., Briggs, D., Eds. *The XPS of Polymers Database*; Surface Spectra, Ltd.: Manchester, U.K., 2000.
(48) Genzer, J.; Kramer, E. J.; Fischer, D. A. Accounting for Auger Yield Energy Loss for Improved Determination of Molecular Orientation Using Soft X-ray Absorption Spectroscopy. *J. Appl. Phys.* **2002**, *92*, 7070−7079.
(49) Fellner-Feldegg, H.; Gelius, U.; Wannberg, B.; Nilsson, A. G.; Basilier, E.; Siegbahn, K. New Developments in ESCA - Instrumentation. *J. Electron Spectrosc. Relat. Phenom.* **1974**, *5*, 643−689.
(50) Ravel, B.; Newville, M. ATHENA, ARTEMIS, HEPHAESTUS: Data Analysis for X-ray Absorption Spectroscopy Using IFEFFIT. *J. Synchrotron Radiat.* **2005**, *12*, 537−541.
(51) Newville, M. IFEFFIT: Interactive XAFS Analysis and FEFF Fitting. *J. Synchrotron Radiat.* **2001**, *8*, 322−324.
(52) Ravel, B. ATHENA User Guide, http://cars9.uchicago.edu/~ravel/software/doc/Athena/html/athena.pdf, 2009.
(53) Seabourne, C. R.; Scott, A. J.; Brydson, R.; Nicholls, R. J. A Systematic Approach to Choosing Parameters for Modelling Fine Structure in Electron Energy-Loss Spectroscopy. *Ultramicroscopy* **2009**, *109*, 1374−1388.
(54) Perdew, J. P.; Burke, K.; Ernzerhof, M. Generalized Gradient Approximation Made Simple. *Phys. Rev. Lett.* **1996**, *77*, 3865−3868.
(55) Monkhorst, H. J.; Pack, J. D. Special Points for Brillouin-Zone Integrations. *Phys. Rev. B: Condens. Matter Mater. Phys.* **1976**, *13*, 5188−5192.
(56) Blaha, P.; Schwarz, K.; Sorantin, P.; Trickey, S. B. Full-potential, Linearized Augmented Plane Wave Programs for Crystalline Systems. *Comput. Phys. Commun.* **1990**, *59*, 399−415.
(57) Moreau, P.; Boucher, F.; Goglio, G.; Foy, D.; Mauchamp, V.; Ouvrard, G. Electron Energy-Loss Spectra Calculations and Experiments as a Tool for the Identification of a Lamellar C_3N_4 Compound. *Phys. Rev. B: Condens. Matter Mater. Phys.* **2006**, *73*, 195111−1−195111−11.
(58) Fucke, K.; Steed, J. W. X-ray and Neutron Diffraction in the Study of Organic Crystal Hydrates. *Water* **2010**, *2*, 333−350.
(59) Taylor, R.; Kennard, O. Comparison of X-ray and Neutron Diffraction Results for the N−H···O═C Hydrogen Bond. *Acta Crystallogr., Sect. B: Struct. Sci.* **1983**, *39*, 133−138.
(60) Parkin, A.; Harte, S. M.; Goeta, A. E.; Wilson, C. C. Imaging Proton Migration from X-rays and Neutrons. *New J. Chem.* **2004**, *28*, 718−721.
(61) Wilson, C. C. *Single Crystal Neutron Diffraction from Molecular Materials*; World Scientific Co. Pte. Ltd.: Singapore, 2000.
(62) Tkatchenko, A.; Scheffler, M. Accurate Molecular van der Waals Interactions from Ground-State Electron Density and Free-Atom Reference Data. *Phys. Rev. Lett.* **2009**, *102*, 073005−1−073005−4.
(63) Broyden, C. G. The Convergence of a Class of Double-Rank Minimization Algorithms 1. General Considerations. *IMA J. Appl. Math.* **1970**, *6*, 76−90.
(64) Fletcher, R. A New Approach to Variable Metric Algorithms. *Comput. J.* **1970**, *13*, 317−322.
(65) Shanno, D. F. Conditioning of Quasi-Newton Methods for Function Minimization. *Math. Comput.* **1970**, *24*, 647−656.
(66) Frisch, M. J.; Trucks, G. W.; Schlegel, H. B.; Scuseria, G. E.; Robb, M. A.; Cheeseman, J. R.; Scalmani, G.; Barone, V.; Mennucci, B.; Petersson, G. A.; , et al., *Gaussian 09*, revision B.01.; Gaussian, Inc.: Wallingford, CT, 2009.
(67) Dennington, R.; Keith, T.; Millam, J. *GaussView*, version 5. ; Semichem Inc., Shawnee Mission, KS, 2009.
(68) Sette, F.; Stöhr, J.; Hitchcock, A. P. Determination of Intramolecular Bond Lengths in Gas Phase Molecules from K Shell Shape Resonances. *J. Chem. Phys.* **1984**, *81*, 4906−4914.
(69) Turci, C. C.; Urquhart, S. G.; Hitchcock, A. P. Inner-Shell Excitation Spectroscopy of Aniline, Nitrobenzene, and Nitroanilines. *Can. J. Chem.* **1996**, *74*, 851−869.
(70) Takahata, Y.; Marques, A. D. S. Accurate Core-Electron Binding Energy Shifts from Density Functional Theory. *J. Electron Spectrosc. Relat. Phenom.* **2010**, *178−179*, 80−87.
(71) Chong, D. P. Density-Functional Calculation of Core-Electron Binding Energies of C, N, O, and F. *J. Chem. Phys.* **1995**, *103*, 1842−1845.
(72) Giesbers, M.; Marcelis, A. T. M.; Zuilhof, H. Simulation of XPS C1s Spectra of Organic Monolayers by Quantum Chemical Methods. *Langmuir* **2013**, *29*, 4782−4788.
(73) Tolbatov, I.; Chipman, D. Performance of Density Functionals for Computation of Core Electron Binding Energies in First-Row Hydrides and Glycine. *Theor. Chem. Acc.* **2014**, *133*, 1473−1−1473−7.
(74) Leon, V.; Parret, R.; Almairac, R.; Alvarez, L.; Babaa, M. R.; Doyle, B. P.; Ienny, P.; Parent, P.; Zahab, A.; Bantignies, J. L. Spectroscopic Study of Double-Walled Carbon Nanotube Functionalization for Preparation of Carbon Nanotube/Epoxy Composites. *Carbon* **2012**, *50*, 4987−4994.